

Article

Analysis of Hydraulic Performance and Flow Characteristics of Inlet and Outlet Channels of Integrated Pump Gate

Chuanliu Xie ^{1,*}, Weipeng Xuan ¹, Andong Feng ¹ and Fei Sun ²¹ College of Engineering, Anhui Agricultural University, Hefei 230036, China² Suqian Branch of Jiangsu Water Source Company of South to North Water Diversion, Suqian 223801, China

* Correspondence: xcltg@ahau.edu.cn

Abstract: The integrated pump gate structure can improve the shortcomings of traditional asymmetric pumping stations with large floor space, but its internal flow mechanism is not clear, which affects its efficient, stable, and safe operation. In order to reveal its internal fluid flow characteristics, numerical simulations based on the N-S equation with the SST $k-\omega$ turbulence model are used in this paper, and experimental validation is carried out. The test results yielded an efficiency of 60.50% near the design flow condition, corresponding to a flow rate of 11.5 L/s, a head of 2.7569 m, a hydraulic loss of 0.064 m in the inlet channel, and a hydraulic loss of 1.337 m in the outlet channel. The integrated pump gate has a uniform inlet water flow pattern, less undesirable flow pattern, and a large backflow vortex in the outlet water. This paper reveals the internal flow characteristics of its integrated pump gate inlet and outlet water, and the research results can provide some reference for the design, theoretical analysis, and application of similar integrated pump gates.

Keywords: integrated pump gate; inlet channel; outlet channel; flow pattern; hydraulic performance



Citation: Xie, C.; Xuan, W.; Feng, A.; Sun, F. Analysis of Hydraulic Performance and Flow Characteristics of Inlet and Outlet Channels of Integrated Pump Gate. *Water* **2022**, *14*, 2747. <https://doi.org/10.3390/w14172747>

Academic Editors: Ran Tao, Changliang Ye and Xijie Song

Received: 28 July 2022

Accepted: 30 August 2022

Published: 2 September 2022

Publisher's Note: MDPI stays neutral with regard to jurisdictional claims in published maps and institutional affiliations.



Copyright: © 2022 by the authors. Licensee MDPI, Basel, Switzerland. This article is an open access article distributed under the terms and conditions of the Creative Commons Attribution (CC BY) license (<https://creativecommons.org/licenses/by/4.0/>).

1. Introduction

In recent years, the frequent occurrence of extreme rainfall weather has posed a serious challenge to the flood control and drainage capacity of cities and towns. In the original pumping station construction, the asymmetric arrangement form is usually used, that is, the combination of sluice gate and pumping station, the gate is set in the middle of the river cross-section direction, and the pump room is set next to the sluice gate. Usually, the area of the water barrier sluice is small, and the pump chambers on both sides cannot pass through the water when no flooding work is needed, resulting in low water exchange efficiency inside and outside the river. At the same time, the construction of a large area of land, long construction period, high economic costs are the traditional pumping station disadvantages. Therefore, the integrated pump and gate device came into being. The integrated pump and gate device is a pumping station that combines a pumping station and a water barrier sluice into a whole arrangement, in which the pump sluice can be used as a water barrier structure instead of a traditional sluice gate, and can provide support for the pump. The pump is arranged on the gate, so there is no need to build a fixed pump room, so that the gate and the pump room are combined into a whole device, which greatly improves the flooding capacity of the river, significantly increases the vitality of the water body in the river channel, and has the advantages of occupying a small area of land compared to traditional pumping stations, short project cycle, lifting and handling, and automatic control, etc., which can also significantly reduce the construction cost, land cost, and alteration cost, and so on, while improving the efficiency of water exchange.

The integrated pump gate consists of sluice gate, gate pump, clapper gate, water stop structure, opening and closing mechanism, etc. Relevant scholars have analyzed its application characteristics and technical advantages, and compared it with traditional pump gate in terms of floor space, circulation, economy, construction cycle, etc. Considering

that integrated pump gates play a significant role in controlling drainage within urban areas and managing black smelly water bodies [1]. Some scholars have discussed their design points and concluded that in urban and rural river management, integrated pump gates will become the mainstream and where the trend of development lies [2]. Some scholars have explored their structures, such as the design of horizontal axial submersible pumps suitable for pump gates [3], to investigate the effects of pump form, installation number, overhang height, pump spacing, and flapper angle on the performance of integrated pump gates [4]. Some other scholars have conducted numerical calculations and model experimental studies on pump gates to derive the stress conditions, flow conditions, and gate vibration characteristics of vertical surface-hole integrated pump gates and horizontal surface-hole integrated pump gates under different operating conditions [5,6]. There is always a negative pressure zone directly below the bottom edge of the flat bottom gate [7], suggesting the two-phase flow and pump gate characteristics in the pump gate pool [8], testing the energy characteristics of the ecological gate pump during bi-directional operation, and resulting in a error of $\pm 2\%$ with the numerical simulation, which verified the reasonableness of the numerical simulation, and finally predicted the optimal installation angle of the vane by numerical simulation [9]. These research results provide basic data for subsequent pump gates selection and other aspects, and also provide reference for subsequent pump gates design and research.

At present, the integrated pump gate has formed a certain scale of industrial system and user demand, but the related research is less, and the flow pattern of the front pool and inlet and outlet water channels is not clear, which limits the further development of the integrated pump gate technology, so it is necessary to carry out further related research, and the research results of this paper have certain theoretical significance and engineering value.

2. Numerical Simulation Model and Method

2.1. Pump Gate Modeling

In accordance with a project pump station design, impeller wood mold diagram, pump gate structure diagram, and other applications of SolidWorks software were used to establish an integrated pump gate model, imported into ANSYS Workbench software [10] in the geometry module for adjustment and boundary condition naming; where model impeller diameter $D = 60$ mm, rotation rate $n = 6692$ r/min, the gate length is 188 mm, width is 60 mm and height is 299 mm, integrated pump gate design flow rate $Q_d = 11.5$ L/s, design head $H = 2.7569$ m. Three-dimensional geometric model of integrated pump gate as shown in Figure 1.

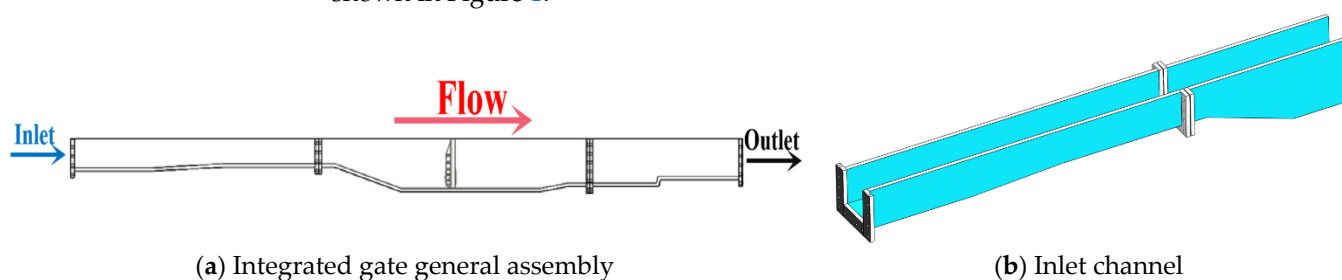


Figure 1. Cont.

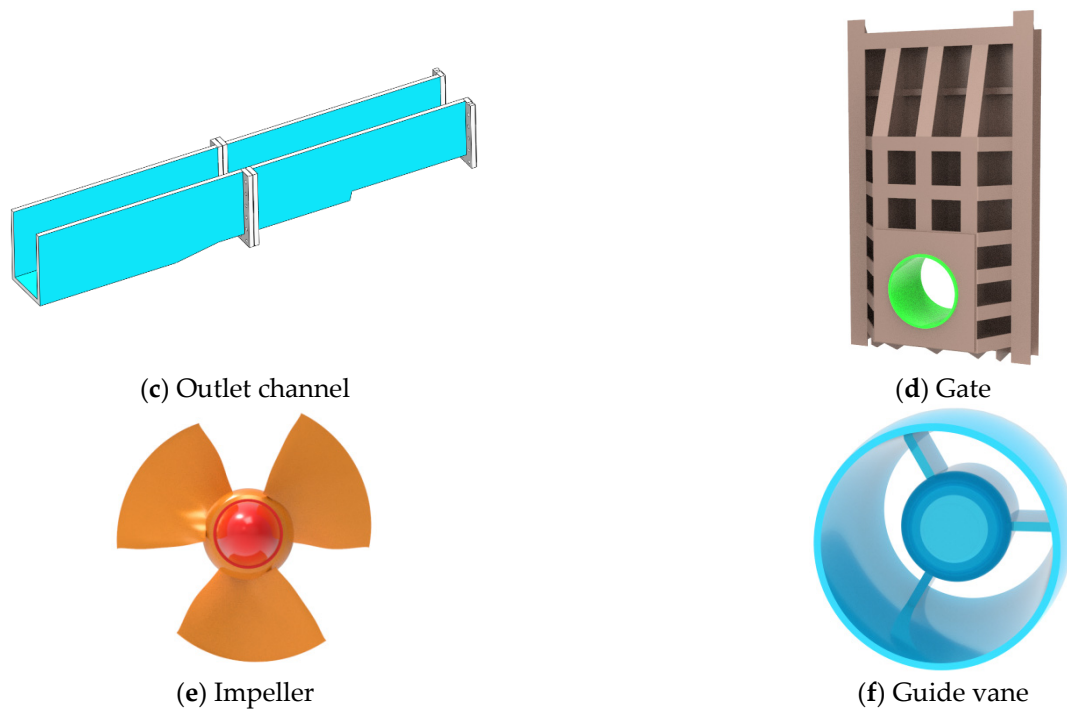


Figure 1. Three-dimensional geometric model of integrated pump gate. (a) Integrated gate general assembly; (b) Inlet channel; (c) Outlet channel; (d) Gate; (e) Impeller; (f) Guide vane.

2.2. Mesh Division

According to the three-dimensional structure of the integrated pump gate, the water overflow part of it is extracted, and the numerical simulation area of the integrated pump gate includes: open inlet channel, gate, impeller, guide vanes, and open outlet channel. In the calculation of this paper, the integrated pump gate is a table-hole type, and in order to better retain the characteristics of the pump gate surface, the model is divided by unstructured mesh, and the number of geometric model meshes is changed under the design flow condition ($Q_d = 11.5 \text{ L/s}$) for mesh-independent analysis. After the grid number reaches 3.03 million, the efficiency of the pump gate basically does not change with the increase of the grid number [11], and this paper determines how to use the grid number of 3.03 million for the subsequent numerical simulation work. Mesh division of each calculation component as shown in Figure 2. The grid-independence results are shown in Figure 3.

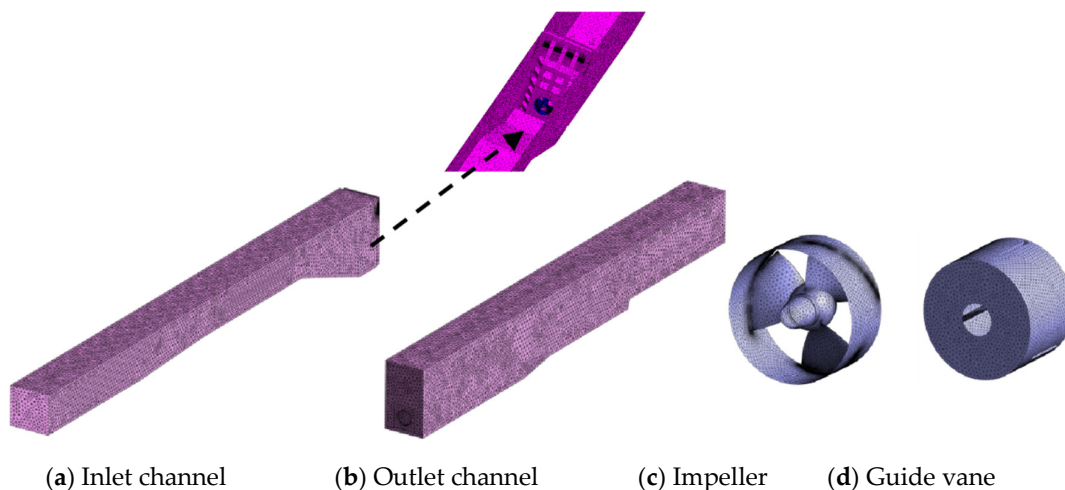


Figure 2. Mesh division of each calculation component.

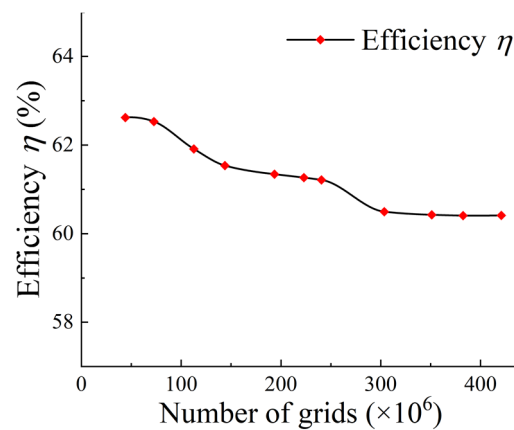


Figure 3. Grid-independent analysis.

2.3. Control Equations, Boundary Conditions, and Calculation Methods

In the numerical simulation of the integrated pump gate, the fluid is treated as a three-dimensional incompressible viscous turbulent flow, without considering heat exchange. Boundary condition settings as shown in Table 1.

Table 1. Boundary condition settings.

Boundary Conditions	Parameter Setting
Inlet	Mass Flow Rate
Outlet	Average Static Pressure
Free liquid level	Symmetry
Dynamic and static interface	Frozen Rotor
Static interfaces	None

In this paper, the SST *k-ω* [12] turbulence model is used to calculate the flow characteristics inside the integrated pump gate, which combines the advantages of the standard *k-ε* model [13] and the standard *k-ω* model [14] and captures the flow in the boundary layer better by using automatic functions in the boundary layer, while the finite element-based finite volume method is used to solve the problem.

In order to evaluate the hydraulic performance of the integrated pump gate after numerical simulation, the hydraulic losses of the inlet and outlet channels, the uniformity of the axial velocity distribution in the characteristic section, the weighted average angle of the velocity in the characteristic section and the energy characteristics of the pump gate were introduced as evaluation bases, and the performance characteristics of the integrated pump gate were evaluated by five quantitative indicators.

In this paper, the total energy difference between the inlet channel of the integrated pump gate and the outlet of the outlet channel is defined as the head of the device and is expressed by the following equation [15]:

$$H_{net} = \left(\frac{\int P_2 u_t ds}{\rho Q g} + H_2 + \frac{\int u_2^2 u_{t2} ds}{2 Q g} \right) - \left(\frac{\int P_1 u_t ds}{\rho Q g} + H_1 + \frac{\int u_1^2 u_{t1} ds}{2 Q g} \right) \quad (1)$$

where the first term on the right side of the equation is the total pressure at the outlet of the outlet channel and the second term is the total pressure at the inlet of the inlet channel.

Where *Q* is the flow rate (m³/s), *H*₁, *H*₂ are the inlet and outlet section elevations of the integrated pump gate (m), *s*₁, *s*₂ for the integrated pump gate inlet and outlet section, *u*₁, *u*₂ for the integrated pump gate inlet and outlet water channel section flow rate at each point (m/s), *u*_{t1}, *u*_{t2} are the normal components of flow velocity (m/s) at each point of the inlet and outlet channel sections of the integrated pump gate, *P*₁, *P*₂ are the static pressure

(Pa) at each point of the inlet and outlet sections of the integrated pump gate, g is the acceleration of gravity (m/s^2).

The efficiency of the integrated pump gate is calculated as [16,17]:

$$\eta = \frac{\rho g Q H_{net}}{T_p \omega} \quad (2)$$

where T_p is the torque (N-m), ω is the rotational angular speed of the impeller. The hydraulic loss h_f is calculated as [18,19]:

$$h_f = E_1 - E_2 = \left(\frac{P_1}{\rho g} - \frac{P_2}{\rho g} \right) + (Z_1 - Z_2) + \left(\frac{u_1^2}{2g} - \frac{u_2^2}{2g} \right) \quad (3)$$

Among them:

$$E_1 = \frac{P_1}{\rho g} + Z_1 + \frac{u_1^2}{2g}; \quad E_2 = \frac{P_2}{\rho g} + Z_2 + \frac{u_2^2}{2g}$$

where E_1, E_2 are the total energy at the inlet and outlet of the open flow channel, P_1, P_2 are the static pressure at the inlet and outlet of the open flow channel (Pa), Z_1, Z_2 are the height of the open flow channel inlet and outlet (m), u_1, u_2 are the open flow channel inlet and outlet velocity (m/s).

The uniformity of flow velocity distribution is calculated as [20]:

$$V_u = \left\{ 1 - \frac{1}{\bar{v}_a} \sqrt{\left[\frac{\sum_{i=1}^n (v_{ai} - \bar{v}_a)^2}{n} \right]} \right\} \times 100\% \quad (4)$$

where, V_u is the uniformity of axial flow velocity distribution in the characteristic section (%), v_{ai} is the axial velocity of each calculation unit (m/s), n is the number of calculation units. The velocity weighted average angle is calculated as [21]:

$$\bar{\theta} = \frac{\sum u_{ai} \left[90^\circ - \arctan \left(\frac{u_{hi}}{u_{ai}} \right) \right]}{\sum u_{ai}} \quad (5)$$

where u_{hi} is the horizontal velocity (m/s) of each unit in the characteristic section of the flow channel. u_{ai} is the axial velocity (m/s) of each calculation unit.

3. Numerical Simulation Results and Analysis

3.1. Hydraulic Performance Results and Analysis

The pressure and torque are extracted from the numerical simulation result file, and the pump gate head is calculated according to equation (1), and the pump gate efficiency is calculated according to equation (2) to obtain the energy performance of the integrated pump gate, as shown in Table 2. The energy performance curve of the integrated pump gate is plotted as shown in Figure 4.

Table 2. Numerical simulation of the energy performance of an integrated pump gate.

Q (L/s)	H (m)	H (%)
8.5 (0.74 Q_d)	3.4884	49.83
9.5 (0.83 Q_d)	3.3126	55.85
10.5 (0.91 Q_d)	3.0206	59.01
11.5 (Q_d)	2.7569	60.50
12.5 (1.09 Q_d)	2.3343	59.73
13.5 (1.17 Q_d)	1.7245	54.87
14.5 (1.26 Q_d)	1.0426	43.58

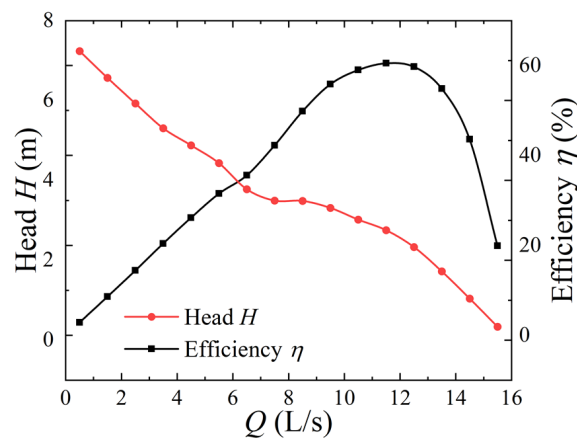


Figure 4. Pump gate energy performance curve.

The calculation results in Table 2 and Figure 4 show that the flow-efficiency curve of the pump gate is approximately quadratic when the inlet water flow is $Q = 0.5\sim 15.5$ L/s, and the head of the pump gate gradually decreases from 7.24 m to 0.34 m, and the efficiency of the pump gate is 60.50% near the design flow condition, the corresponding flow is 11.5 L/s and the head is 2.7569 m. When the flow rate is 10.5~12.5 L/s ($0.91\sim 1.09 Q_d$), the pump gate is in the high efficiency zone, and the efficiency of the pump gate is around 59~60%. When the flow rate is 5.5~7.5 L/s ($0.48\sim 0.65 Q_d$), the pump gate is located near the saddle area, and the operation of the pump gate is not stable at this time, so it is recommended to avoid operating in this flow range.

3.2. Analysis of Internal Flow in Inlet Channel

An axial section was created using the impeller rotation axis as a reference to explore the internal flow characteristics of the inlet flow channel before the pump gate. The schematic diagram of the axial section is shown in Figure 5.

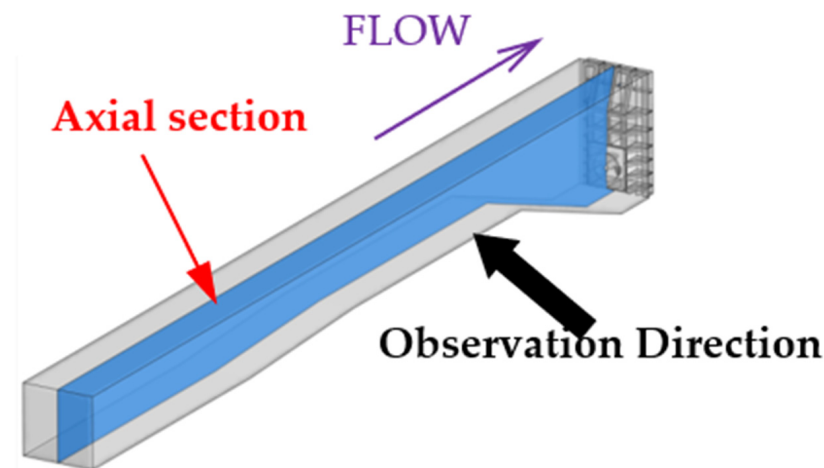


Figure 5. Schematic diagram of the axial section of the open inlet channel.

3.2.1. Inlet Channel Streamline and Axial Flow Velocity Distribution

The streamline and axial flow velocity distribution clouds of the open inlet channel under different flow conditions in the section are drawn, as shown in Figure 6.

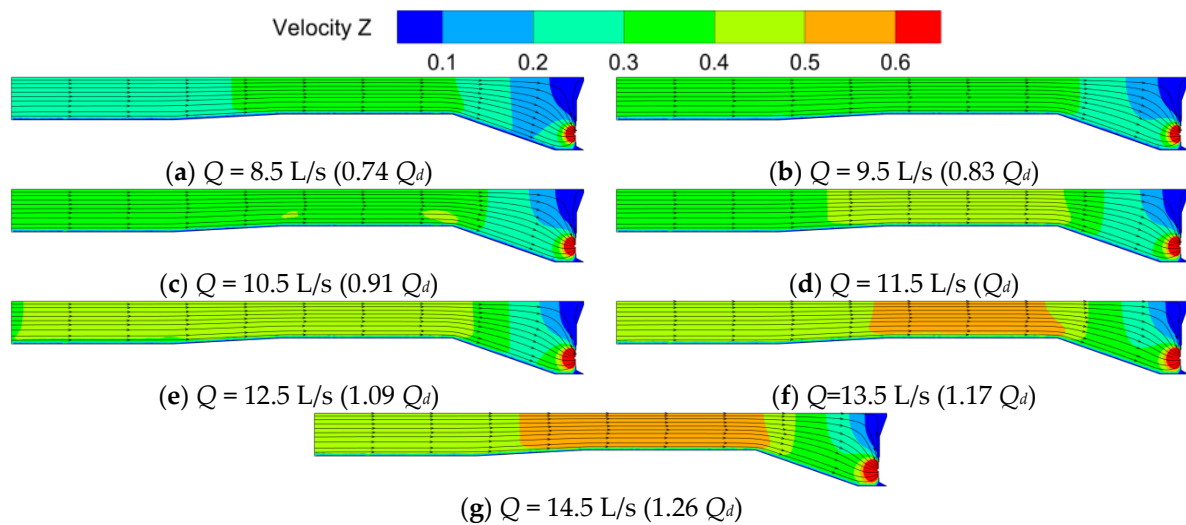


Figure 6. Cloud diagram of inlet channel streamline and axial flow velocity distribution under different working conditions.

Through the analysis of Figure 6, it is concluded that under different flow conditions, the streamline of open inlet channel is smooth, contraction is reasonable, and the streamline is regular, which can provide better water inlet conditions for the impeller. The slope of the open inlet channel is not easy to be too large, as too large will not only lead to aggregation of water flow, but also very easy to form vortex at the bottom, hence should be avoided; the figure can be found in the inlet channel of the slope of the decline is reasonable, no bad flow conditions.

Under each flow condition ($Q = 8.5\sim 14.5 \text{ L/s}$), the flow velocity increases in the direction from the inlet of the inlet channel to the inlet of the pump gate; at the top of the pump gate structure, there is a low velocity zone because the water flow receives the constraint of the pump gate; the water flow gathers at the inlet of the pump because of the negative pressure created when the pump rotates, and the flow velocity reaches the maximum value here, which is greater than 0.6 m/s . The flow velocity at the inlet of the pump gate varies in a uniform gradient. Under the design condition ($Q = 11.5 \text{ L/s}$), the velocity field is the most uniform in the inlet channel, and under low and high flow conditions, the high and low velocity areas are mixed more obviously.

The local area from the slope of the inlet channel to the inlet of the pump gate is extracted separately as a research object, and the streamline and pressure distribution clouds at the inlet of the pump gate of the open inlet channel under different flow conditions are drawn in the section, as shown in Figure 7.

It can be concluded from Figure 7 that with the increase of flow rate ($Q = 8.5\sim 14.5 \text{ L/s}$), the static pressure in the inlet channel is gradually increasing, and under the design condition ($Q = 11.5 \text{ L/s}$), the pressure at the bottom of the slope to the pump inlet is approximately the same, and the pressure only starts to decrease in front of the pump gate impeller inlet, under the high flow rate and low flow rate conditions, the pressure gradient near the pump gate inlet is large and the pressure gradually decreases, the pressure is lowest at the inlet of the pump gate.

3.2.2. Hydraulic Loss of Inlet Channel

According to the Formula (3) to calculate the inlet channel hydraulic loss, drawing different flow conditions in the inlet channel hydraulic loss curve, as shown in Figure 8.

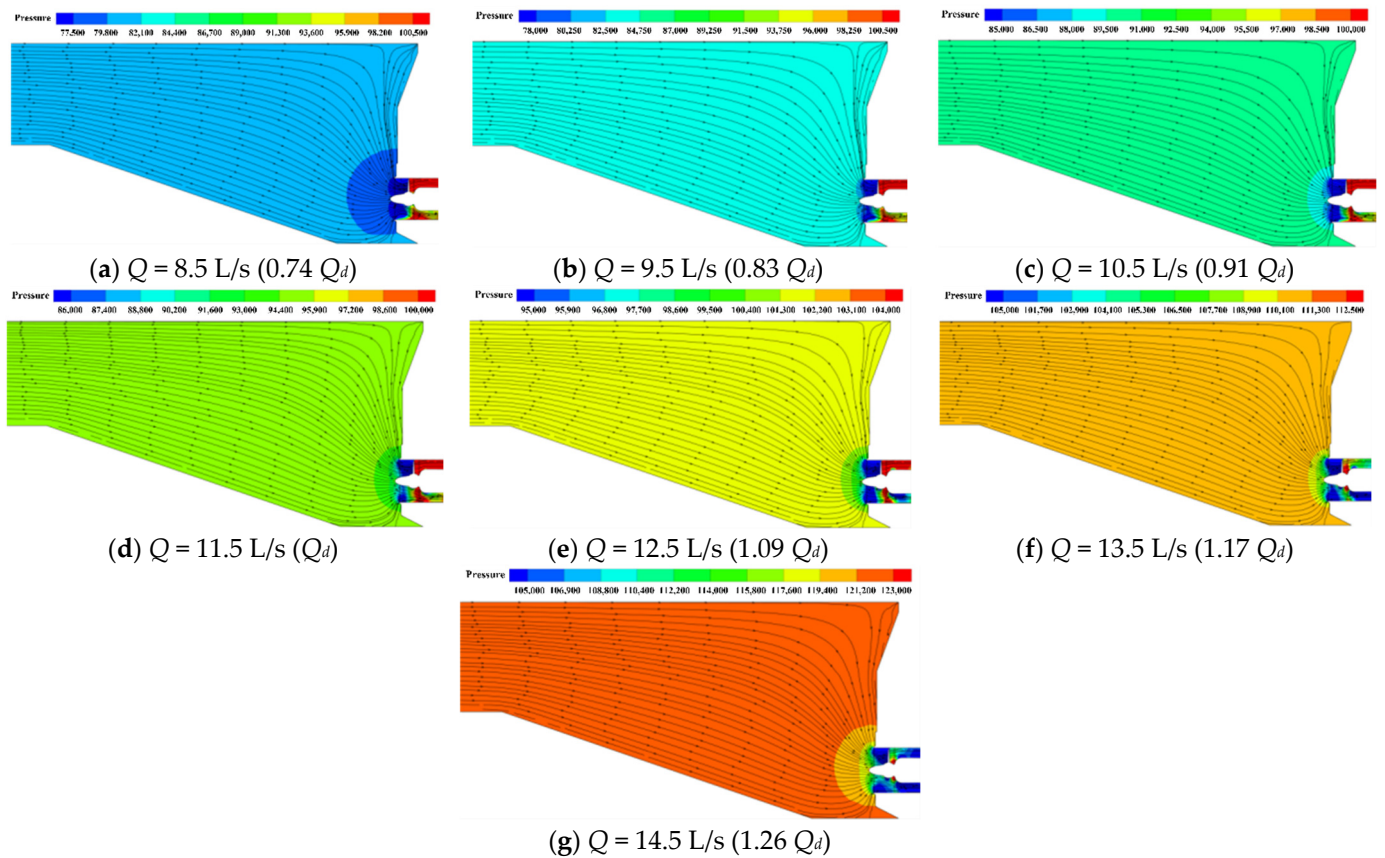


Figure 7. Cloud diagram of streamline and pressure distribution at the inlet of pump gate under different working conditions.

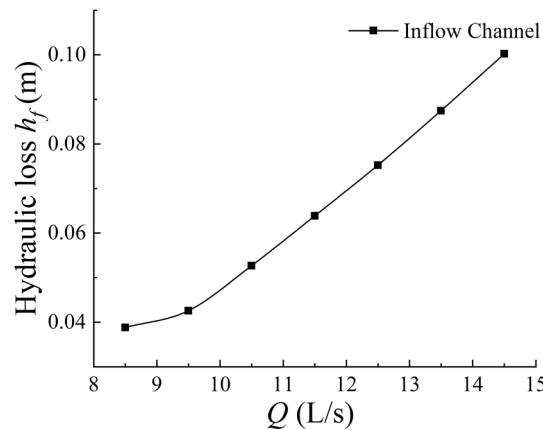


Figure 8. Hydraulic loss curve of inlet channel under different working conditions.

The analysis of Figure 8 shows that the hydraulic loss of the inlet channel h_f is positively correlated with the flow rate Q , which approximately satisfies the quadratic function, and the hydraulic loss is the smallest when the inlet flow rate is 8.5 L/s ($0.74 Q_d$), which is 0.039 m, and the largest when the flow rate is 14.5 L/s ($1.26 Q_d$), which is 0.100 m. The larger the flow rate, the larger the hydraulic loss, and in this type of pump station, the hydraulic loss of the inlet and outlet channels is a decisive factor in the efficiency of the pump gate. The calculation results show that the average level of hydraulic loss of the inlet channel is about 6 cm, which is in line with the conventional theory and design.

3.3. Analysis of Internal Flow in Outlet Channel

An axial section is created with the impeller rotation axis to observe the flow characteristics in the outflow channel. The schematic diagram of the axial section is shown in Figure 9.

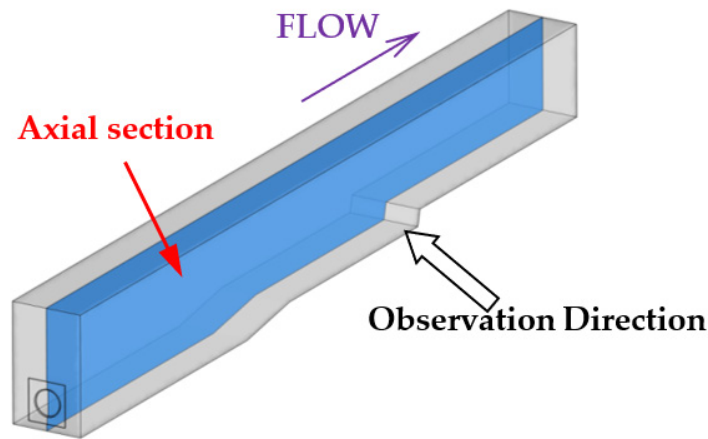


Figure 9. Schematic diagram of axial section of open outlet channel.

3.3.1. Streamline and Axial Velocity Distribution of Outlet Channel

The streamline and axial flow velocity distribution clouds of the open outlet channel under different flow conditions in the section were drawn, as shown in Figure 10.

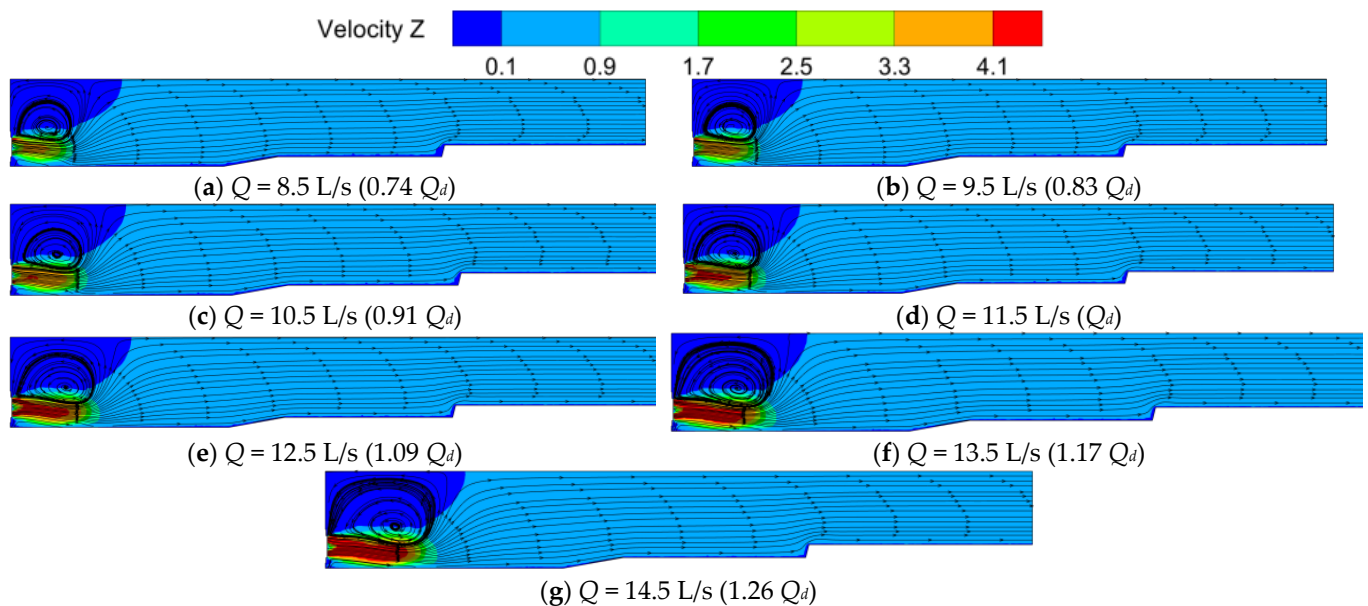


Figure 10. Streamline and axial velocity distribution of the outlet channel under different flow conditions.

It can be found in Figure 10 that the outflow channel is turbulent near the pump gate, and a return vortex parallel to the flow direction is formed at the outlet of the pump gate guide vane, and the size of the vortex increases as the flow rate increases. When the flow rate is 8.5~10.5 L/s (0.74~0.91 Q_d), the axial flow velocity at the outlet of the pump gate is about 3.3 m/s; when the flow rate is 11.5~14.5 L/s (Q_d ~1.26 Q_d), the axial flow velocity at the outlet is about 4.1 m/s, and then there is a step transition along the outlet direction, due to the existence of vortex, the axial flow velocity above the pump gate is lower. The axial flow velocity above the outlet is low. The existence of the vortex is mainly due to the open outlet upper part of the stagnant water area, where the flow velocity is low due to

the rotation of the impeller, the lower and middle water flow velocity is fast, making the formation parallel to the direction of the water flow back vortex.

The local flow field at the outlet of the pump gate is taken out, and the streamline and pressure distribution clouds at the outlet of the pump gate of the open outflow channel under different flow conditions in the section are drawn, as shown in Figure 11.

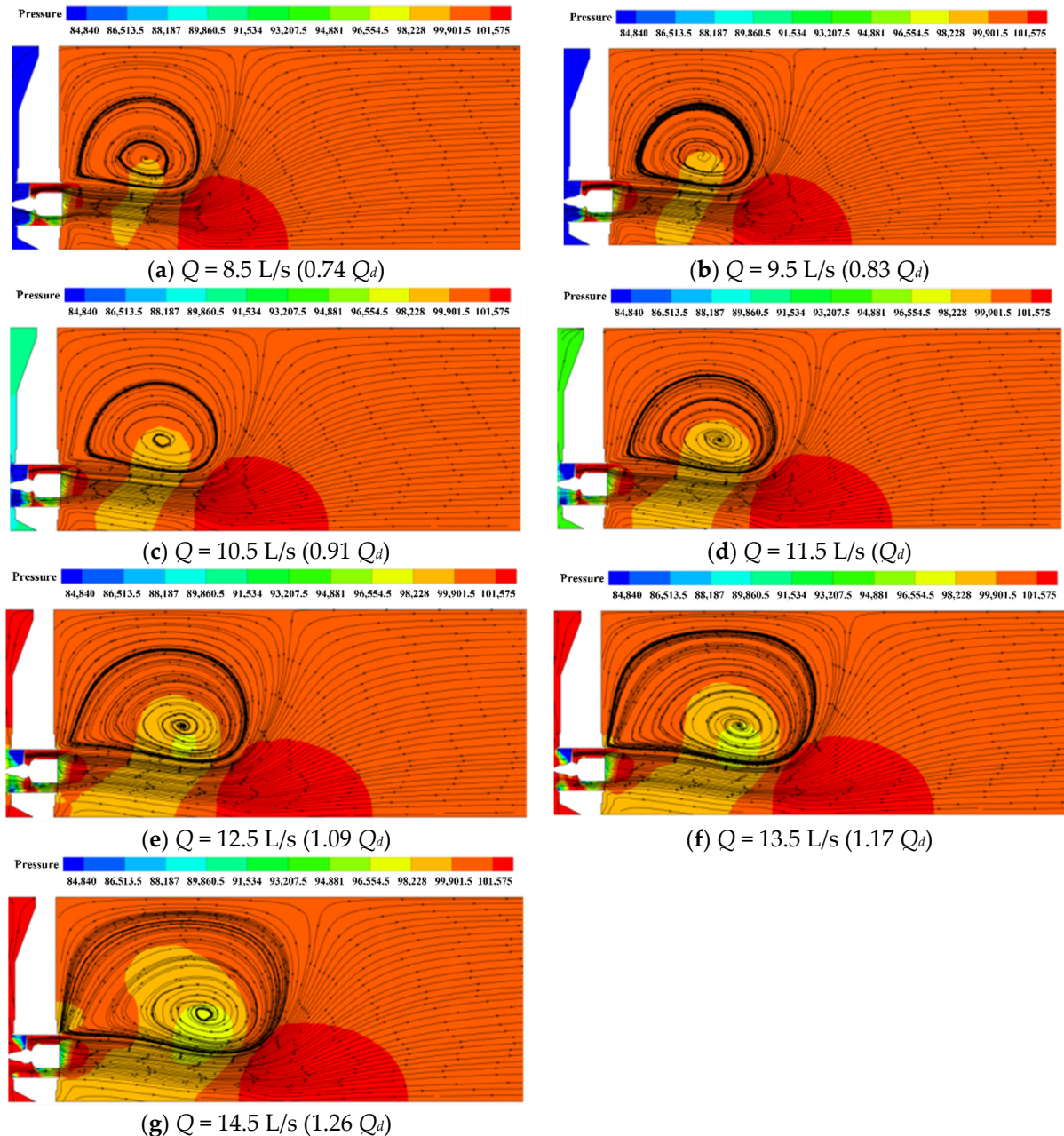


Figure 11. Streamline and pressure distribution at the pump gate outlet under different flow conditions.

As can be seen from Figure 11, at different flow rates, there is a backflow vortex above the pump gate outlet. With the increase of flow rate, the size of the vortex area also increases, and the center of the backflow vortex also shifted to the outlet of the outflow channel. Under the action of gravity, the fluid flows as a whole to the bottom of the pool to do offset flow, and due to the existence of vortex, the pressure at the outlet is low, and with the increase of vortex, the low pressure area also increases; pump gate outlet is 5~9 D at the bottom of the pool, and there is a semicircular piece of high pressure area, and due to the

slope of the outflow channel, the pressure returns to normal level, and the streamline also began to level off.

3.3.2. Hydraulic Loss of Outlet Channel

According to the Formula (3) to calculate the hydraulic loss of the outlet channel, draw the hydraulic loss curve of the outlet channel under different flow conditions, as shown in Figure 12.

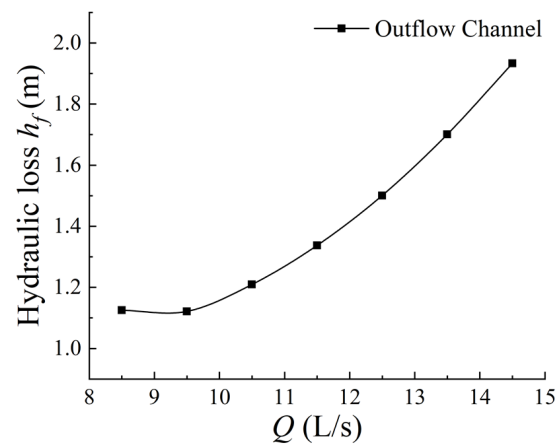


Figure 12. Hydraulic loss curve of outlet channel under different working conditions.

As can be seen from Figure 12, the hydraulic loss of the open outlet channel under different flow conditions is approximately parabolic with an open upward distribution, reaching a minimum value of 1.121 m at an inlet flow rate of 9.5 L/s ($0.83 Q_d$). With the increase of the inlet flow rate, the hydraulic loss also gradually increases, reaching a maximum value of 1.933 m at an inlet flow rate of 14.5 L/s ($1.26 Q_d$).

3.4. Three-Dimensional Flow Regime Analysis

3.4.1. Integrated Pump Gate Three-Dimensional Streamline and Characteristic Cross-Sectional Flow Rate

The characteristic section is shown schematically in Figure 13, the specific location is shown in Table 3, and the pump gate impeller diameter $D = 60$ mm.

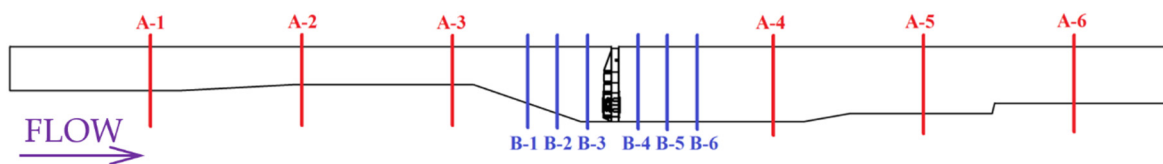


Figure 13. Schematic diagram of the characteristic cross section.

Setting characteristic sections A-1, A-2, A-3 in order at $10 D$ intervals from the impeller inlet. Setting characteristic sections A-4, A-5, A-6 in order at $10 D$ intervals from the guide vane outlet. Setting characteristic sections B-1, B-2, B-3 in order at distances $5 D$, $3 D$ and D from the impeller inlet. Setting characteristic sections B-4, B-5, B-6 in order at distances D , $3 D$ and $5 D$ from the guide vane outlet.

The position of $5 D$, $3 D$, D from the impeller inlet and D , $3 D$, $5 D$ from the guide vane outlet are selected to make cross sections, and the sections are shown in the characteristic sections B-1~B-6 in Figure 13, and the three-dimensional streamlines and axial flow velocity distribution of the integrated pump gate in the characteristic sections are shown in Figures 14–20.

Table 3. Summary of characteristic selections.

Characteristic Section Number	Distance from Impeller Inlet L_1	Distance from Guide Vane Outlet L_2
A-1	$30 D$	
A-2	$20 D$	
A-3	$10 D$	
A-4		$10 D$
A-5		$20 D$
A-6		$30 D$
B-1	$5 D$	
B-2	$3 D$	
B-3	D	
B-4		D
B-5		$3 D$
B-6		$5 D$

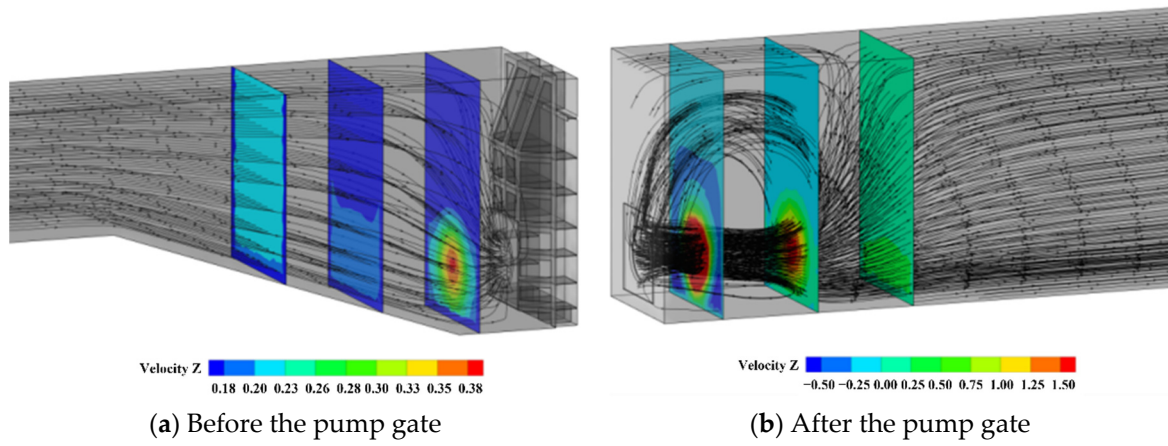


Figure 14. $Q = 8.5 \text{ L/s}$ ($0.74 Q_d$).

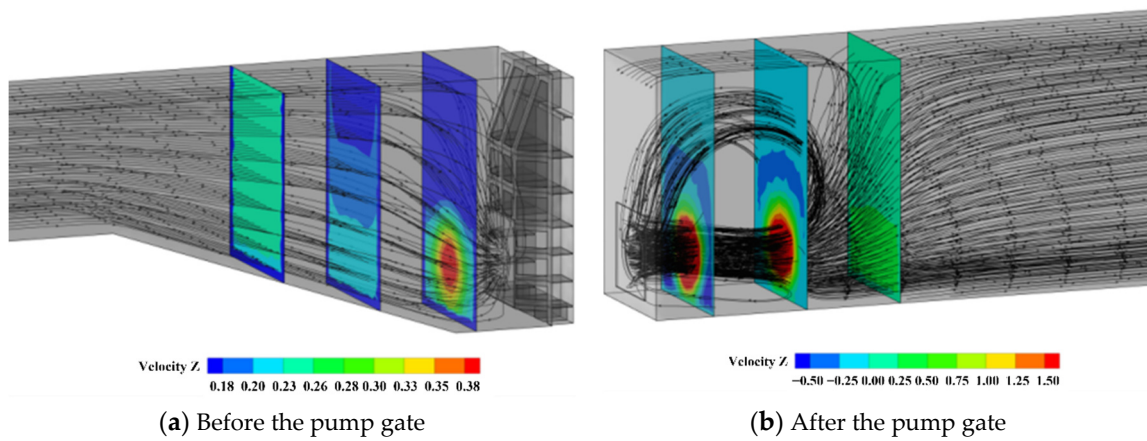


Figure 15. $Q = 9.5 \text{ L/s}$ ($0.83 Q_d$).

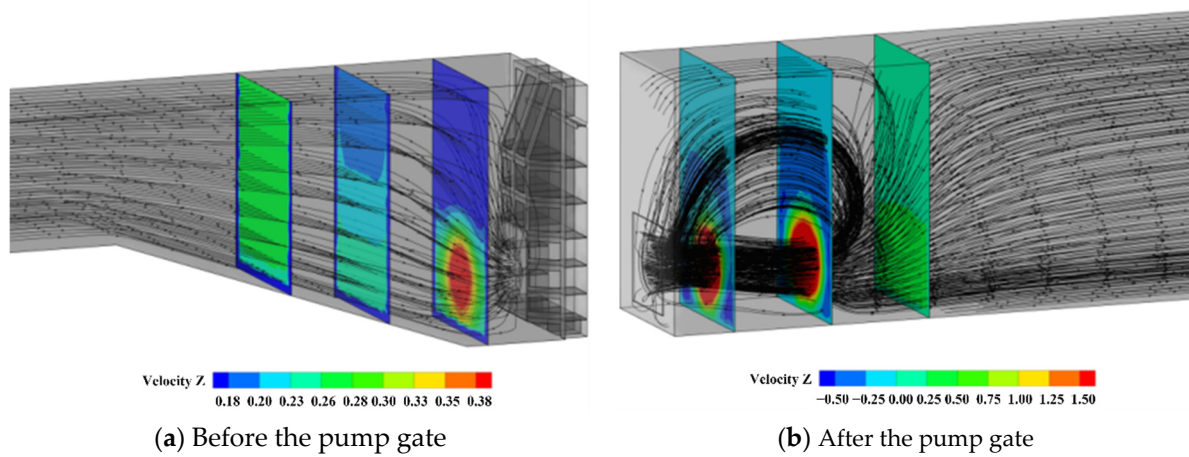


Figure 16. $Q = 10.5 \text{ L/s}$ ($0.91 Q_d$).

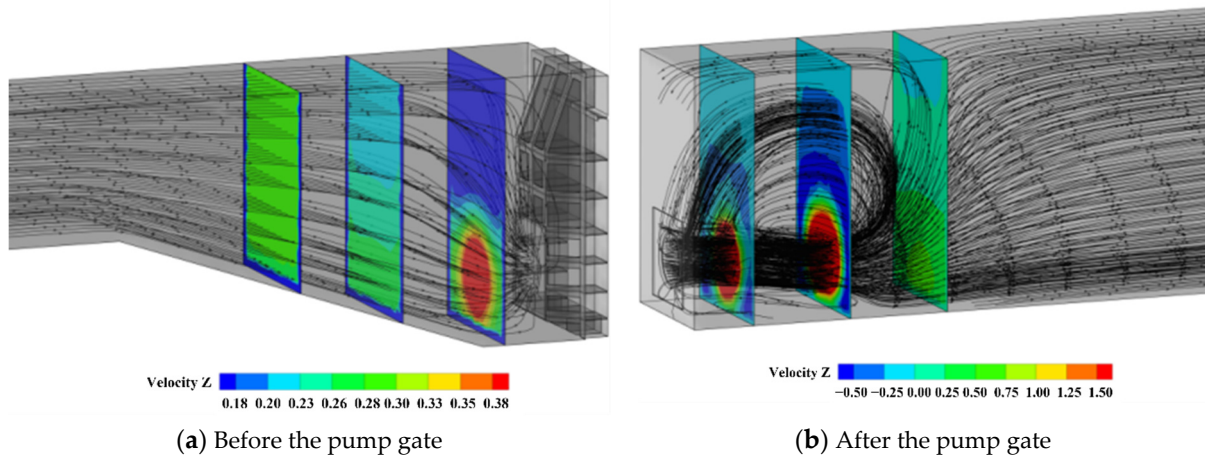


Figure 17. $Q = 11.5 \text{ L/s}$ (Q_d).

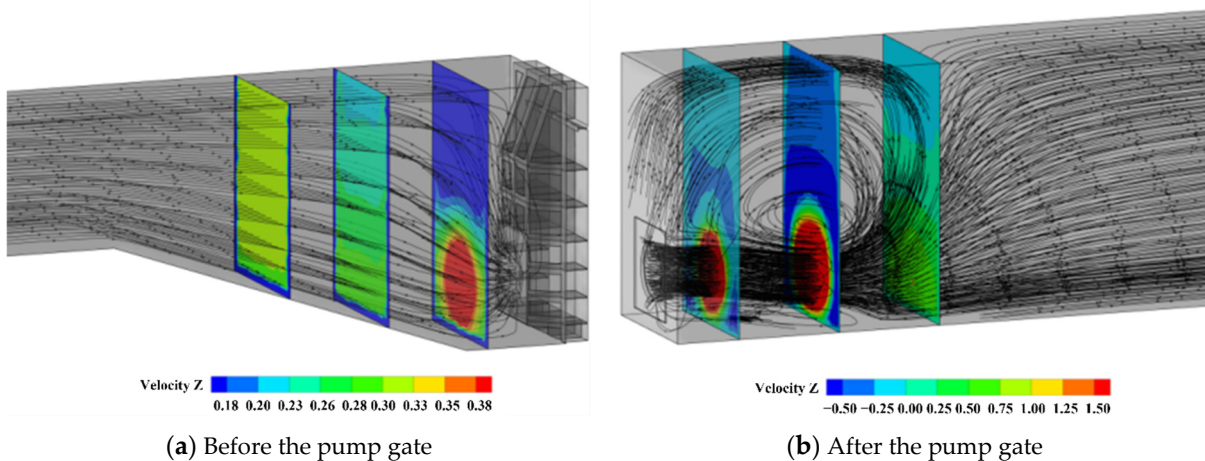


Figure 18. $Q = 12.5 \text{ L/s}$ ($1.09 Q_d$).

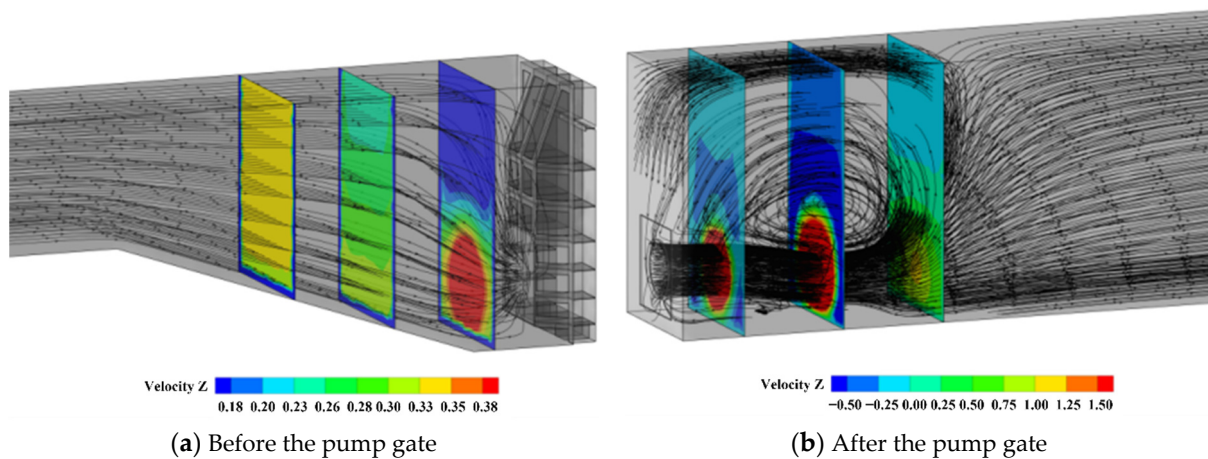


Figure 19. $Q = 13.5 \text{ L/s}$ ($1.17 Q_d$).

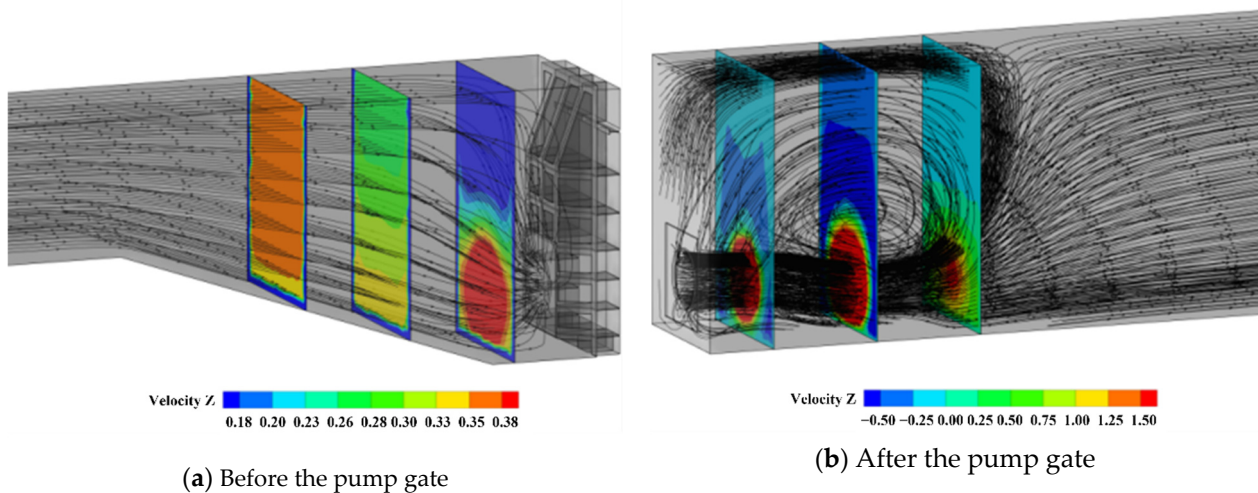


Figure 20. $Q = 14.5 \text{ L/s}$ ($1.26 Q_d$).

By comparing Figures 14 and 20, it can be seen that before the impeller inlet of the pump gate, with the increase of the inlet flow rate, there is no adverse flow pattern in the inlet channel, and the streamlines are uniformly contracted toward the impeller inlet. Comparing the axial velocity distribution clouds in the sections at different flow rates, it can be seen that the axial velocity in the same sections gradually increases with the increase of the inlet flow rate. At $5 D$ from the impeller inlet, the axial velocity distribution in the section is more uniform, and the velocity at the side wall is smaller due to the boundary layer effect. At $3 D$ from the impeller inlet, the velocity in the section gradually increases from top to bottom, which is mainly due to the slope that causes the water to collect at the bottom of the pool. At the impeller inlet D , the axial flow velocity is distributed outward in a circular pattern, and the high velocity area is located in the lower and middle part of the slice at the level of the impeller, while the flow velocity in the upper and middle part of the section is lower.

From the distribution of streamlines in the outlet section of Figures 14 and 20, it can be concluded that between $3 D$ and $5 D$ from the guide vane outlet, there is separation and stratification of the fluid caused by vortices, which is due to the opposite axial flow velocity of the streamlines. The region of high flow velocity within each section is located in the middle and lower part, and the axial flow velocity of the water in the middle and upper part is opposite to the flow velocity at the bottom of the flow channel due to the presence of vortices. At D and $3 D$ from the guide vane outlet, the axial flow velocity in the sections is distributed in a circular band, decreasing from the center line of the guide vane to the top and bottom of the sections. At $5 D$ from the guide vane outlet, when the flow

rate is 8.5~13.5 L/s (0.74~1.17 Q_d), the axial flow velocity in the sections is approximately the same, and only the upper part of the sections is slightly lower. When the flow rate is 14.5 L/s (1.26 Q_d), there is still a circular region of high axial velocity in the section, which is caused by the fact that as the flow rate increases, the flow rate increases and the high velocity region also shifts toward the outlet of the outflow channel. At a flow rate of 8.5 L/s (0.74 Q_d), the area of the high flow velocity region in the slice at D from the guide vane outlet is larger than that in the slice at 3 D from the guide vane outlet, and the area of the high flow velocity region in the slice at 3 D from the guide vane outlet is larger than that in the slice at D from the guide vane outlet for the rest of the flow conditions, This is due to small flow conditions, small flow rate, short distance of high-speed water flow transmission at the outlet of pump gate, and fast dissipation of kinetic energy.

3.4.2. Uniformity of Axial Flow Velocity Distribution and Velocity-Weighted Average Angle of Each Characteristic Section under Design Conditions

Through the CFD-post post-processing interface, the velocity components of each unit in the characteristic section are derived, and the axial velocity components are extracted, and the axial velocity distribution uniformity and velocity-weighted average angle of each characteristic section are calculated in turn, according to Formulas (4) and (5), as shown in Table 4, where the characteristic sections B-4, B-5, and B-6 are closer to the guide vane outlet, and the water flow is not fully diffused, and their the axial velocity distribution uniformity and velocity weighted average angle are not very meaningful, so they are not selected. The axial velocity distribution uniformity and velocity-weighted average angle curves of each characteristic section under different flow conditions are plotted as shown in Figure 21.

Table 4. Uniformity of axial flow velocity distribution and velocity-weighted average angle for each characteristic section under design condition.

Evaluation Indicators	Section A-1	Section A-2	Section A-3	Section B-1	Section B-2	Section B-3	Section A-4	Section A-5	Section A-6
Uniformity of flow rate distribution V_u (%)	95.42	94.18	93.95	96.72	91.15	45.33	95.37	98.26	98.25
Velocity – weighted average angle $\bar{\theta}$ (°)	89.93	89.71	89.54	79.47	75.30	62.01	87.95	89.67	89.96

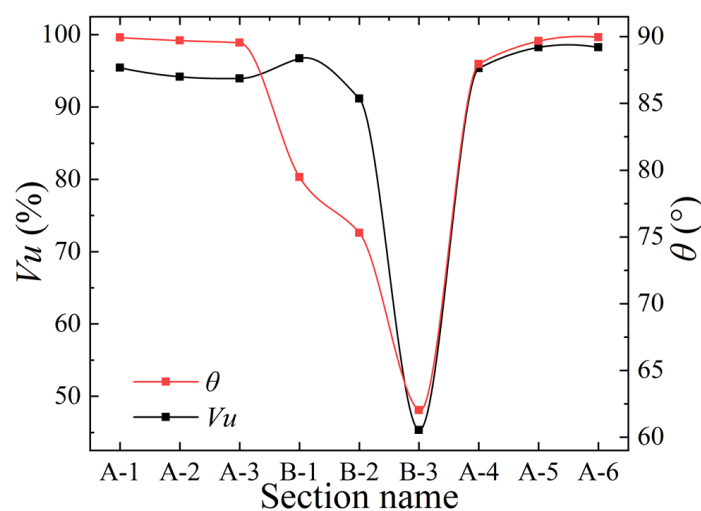


Figure 21. The uniformity of axial flow velocity distribution and velocity-weighted average angle curve of each characteristic section.

The more uniformity of axial flow velocity distribution is close to 100%, it means that the more uniform flow velocity in the section, by comparing the uniformity of axial flow velocity distribution in each characteristic section, it can be seen that the uniformity of axial flow velocity distribution in section B-2 and section B-3 is slightly lower under the design working condition. At section B-1, the inlet slope is more reasonable, and the uniformity of axial flow velocity distribution can reach 96.72%, as section B-2 and section B-3 are close to the impeller inlet. Influenced by the suction of the pump gate, the high-speed zone is concentrated in the axial direction of the impeller of the pump gate, the flow velocity gradually decreases in the axial direction in the shape of a ring around, the axial flow velocity distribution is first reduced to 91.15% (B-2), and then reduced to 45.33% (B-3), the closer to the pump gate inlet flow velocity uniformity is lower, from Figures 14–20 can also find this phenomenon. In the outlet channel, the uniformity of axial velocity distribution gradually increases, reaching 98.25% at section A-6, which indicates that the water flow diffusion is reasonable and the flow pattern affected by pump gate recovers quickly.

The closer the velocity-weighted average angle is to 90° , the better the isotropy of the water flow. By comparing the velocity-weighted average angle of each characteristic section, it can be seen that the velocity-weighted average angle decreases slightly at section A-1, section A-2, and section A-3, which is approximately a primary function relationship, and there is no obvious decrease. The velocity isotropy is better. At sections B-1, B-2, and B-3 near the impeller inlet, the velocity-weighted average angle decreases to 79.47° , 75.30° , and 62.01° respectively, and the closer to the pump gate, the smaller the velocity-weighted average angle is, which is also due to the influence of the high speed rotation of the pump gate, resulting in the velocity-weighted average angle in the section near the pump gate impeller is obviously different from other parts of the characteristic section. The velocity-weighted average angle in the section near the impeller of the pump gate is significantly different from that in other parts of the characteristic section. In the outflow channel, the velocity-weighted average angle gradually increases and reaches 89.96° at section A-6, indicating that the isotropy of the flow has been restored.

4. Internal Flow Characteristics Test Analysis

4.1. Introduction to the Pump Gate Test Rig

The total length of the test bench is about 7.5 m, the total width is about 1.8 m, and the diameter of the circulating pipe is 0.1 m. The test bench is made of transparent plexiglass, which can help visually and clearly observe the flow pattern of the inlet and outlet water channels of the pump gate, the position of the vortex, and the distribution of the bad flow pattern. The two-dimensional schematic, three-dimensional rendering and real objects of the test bench are shown in Figures 22 and 23 respectively, and the test measuring instruments and equipment are shown in Table 5.

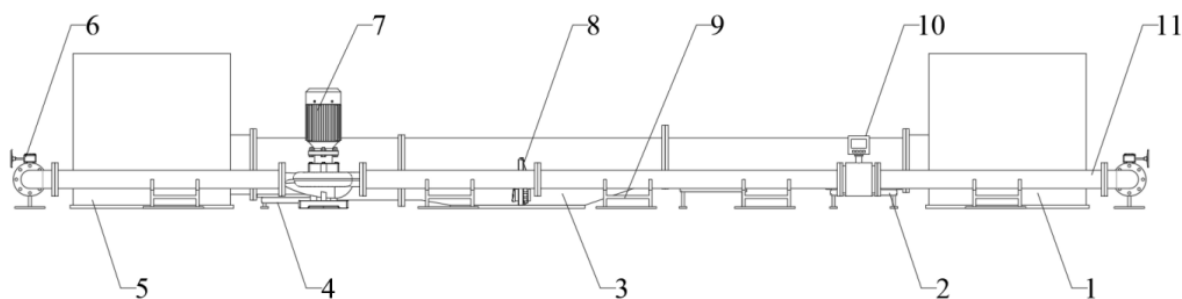


Figure 22. Schematic diagram of test bench: 1. water inlet tank; 2. water inlet channel support part; 3. open inlet and outlet channels; 4. outlet channel support part; 5. outlet water tank; 6. flange butterfly valve; 7. booster pump; 8. tested integrated pump gate; 9. pipe support; 10. electromagnetic flowmeter; 11. circulating pipeline.

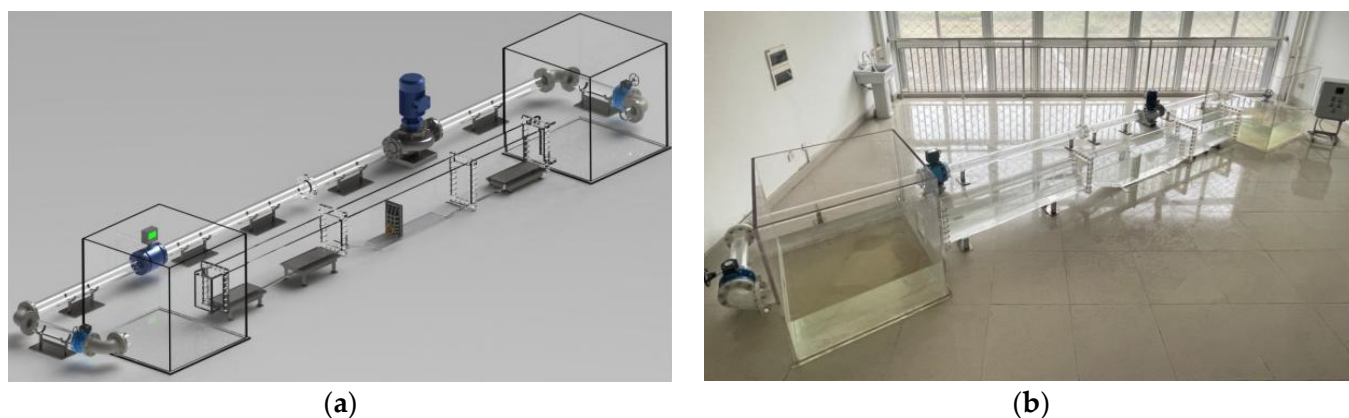


Figure 23. Three-dimensional rendering drawing and physical drawing of integral pump gate test stand: (a) Three-dimensional rendering drawing of integrated pump gate test stand; (b) physical drawing of integrated pump gate test stand.

Table 5. Main instruments and equipment for test data acquisition.

Measurement Items	Name of Measuring Equipment	Model	Scope of Work	Accuracy
Flow rate	Electromagnetic flow meters	ZEF-DN100	0~120 m ³ /h	±0.5%
Rotational speed	Laser tachographs	DT-2234C	0.1~99,999 r/min	±0.05%
Flow pattern	High-speed cameras	OLYMPUS i-SPEED 3	2000 fps Full resolution Maximum 15,0000 fps	±1 μs

4.2. Test results and Analysis

4.2.1. Analysis of Flow Characteristics of Open Inlet and Outlet Water Channels

(1) Flow characteristics of open inlet channels

In this paper, the oscillation of the tracer red line is used to reflect the flow characteristics of the inlet channel. The flow patterns at positions A-1, A-2, and A-3 at the design flow rate $Q = 11.5 \text{ L/s}$ (Q_d) are selected for analysis by means of a high-speed camera, as shown in Figure 24.

From the tracer red lines in Figure 24, it can be seen that the water flow in the characteristic sections A-1, A-2, and A-3 is smooth, the streamline of the rear side wall of the characteristic section A-1 is evenly spaced, and the tracer red lines are parallel to each other, without cross winding. The tracer red line on the bottom rises slightly and floats upward, which is caused by the slope at the rear of section A-1, similar to the streamline state obtained in numerical simulation, the results of axial velocity distribution uniformity and velocity weighted average angle at this position can also show that the flow pattern here is smooth and the streamline is uniform. There is a horizontal flow passage between section A-2 and section A-3, and the streamline of this section remains horizontal, and the tracer red line does not appear disorderly and staggered, which is similar to the streamline diagram obtained by numerical simulation (Figure 6).

(2) Flow characteristics of open outlet channels

The flow characteristics of the water channel are reflected by the oscillating attitude of the tracer red line. The flow pattern is captured by a high-speed camera and selected for analysis at positions A-4, A-5, and A-6 at a design flow rate of $Q = 11.5 \text{ L/s}$ (Q_d), as shown in Figure 25.

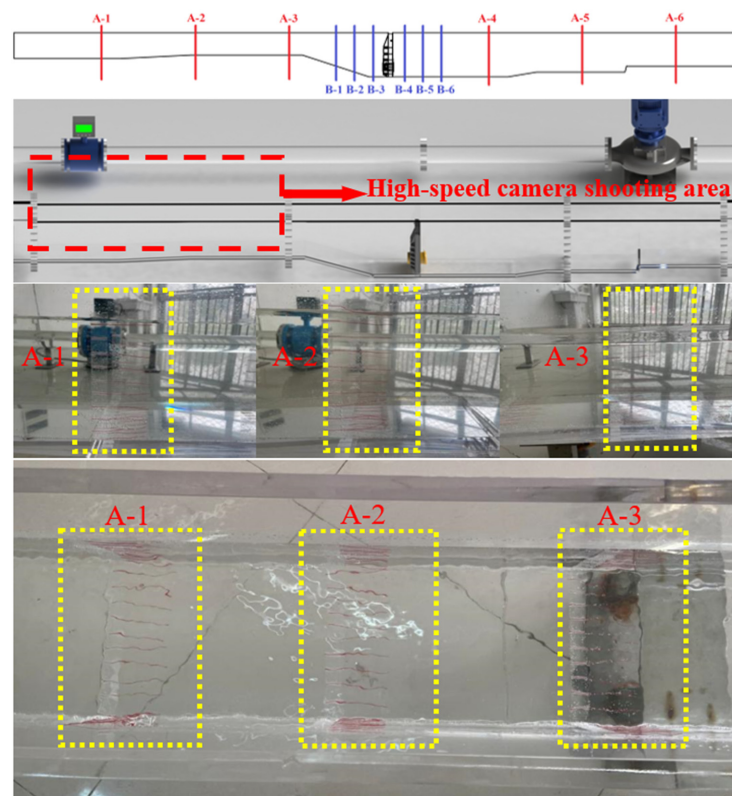


Figure 24. Flow pattern in an open inlet channel.

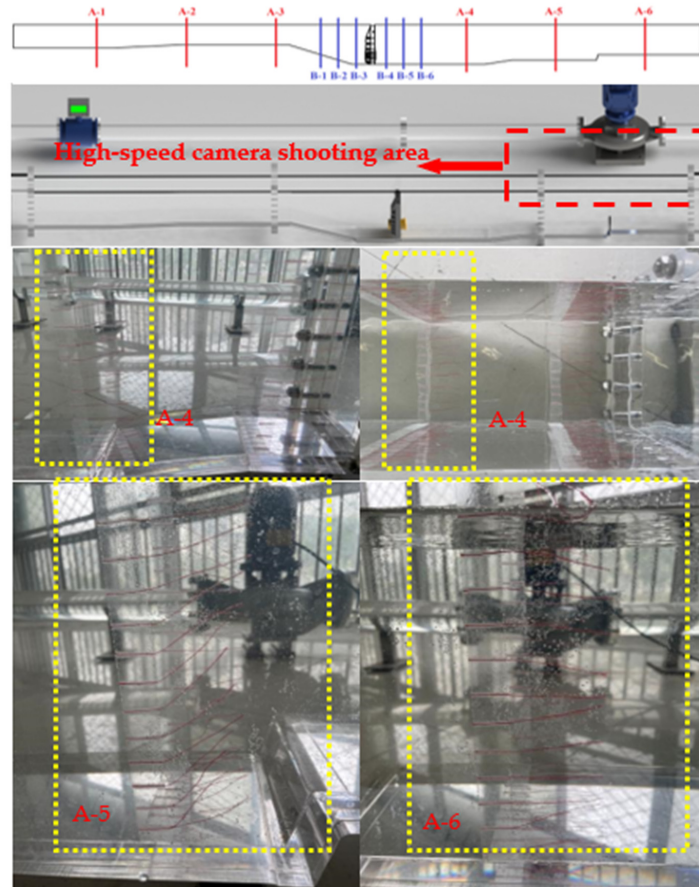


Figure 25. Flow pattern in an open outlet channel.

From the tracer red line in Figure 25, it can be seen that in the outlet channel, the streamline near the characteristic section A-4 is smooth, and the tracer red line on the wall and bottom slightly swings upward under the action of the rear slope of section A-4, which is similar to the phenomenon obtained by numerical simulation. At the characteristic section A-5, due to the existence of the outlet slope, the tracer red line swings up significantly, but before reaching the characteristic section A-6, the tracer red line has recovered to the level, which is similar to the streamline in the numerical simulation (Figure 10). This phenomenon can also be verified by comparing the weighted average angles of the two sections in Table 4 and Figure 21.

4.2.2. Analysis of the Flow Characteristics at the Inlet and Outlet of the Pump Gate Impeller

(1) Flow characteristics at the inlet of the pump gate impeller

As shown in Figure 26, by observing the tracer red line at the impeller inlet of the pump gate design flow $Q = 11.5 \text{ L/s}$ (Q_d), it can be found that the tracer red line converges to the impeller rotation center under the action of low pressure at the impeller inlet of the pump gate, gradually shrinks and swings evenly, there is no cross wrapping at the pump shaft, and the tracer red line at the upper part of the inlet channel faces the pump inlet, which is similar to the numerical calculation result (Figure 6), the slope of the inlet passage provides good inlet conditions for the impeller.

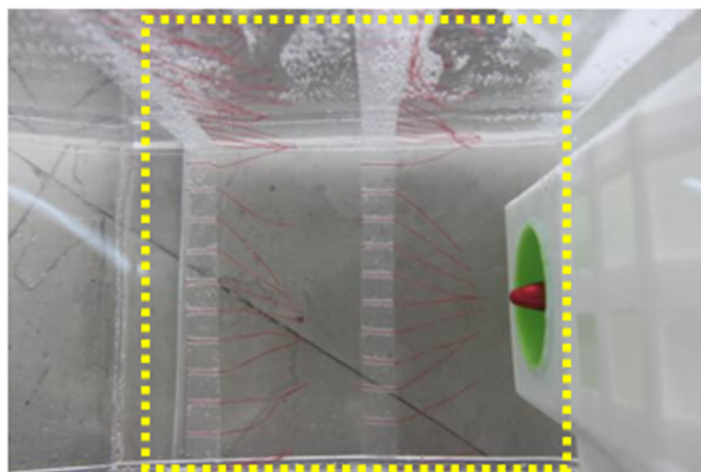


Figure 26. Flow pattern at pump gate impeller inlet.

(2) Flow characteristics at the outlet of the pump gate guide vane

As shown in Figure 27, the design flow rate of the pump gate $Q = 11.5 \text{ L/s}$ (Q_d) can be obtained through the test, and there is an obvious backflow vortex at the outlet of the guide vane, section B-4, the side wall against the lower and bottom tracer red line swing toward the outflow channel, the side wall against the upper tracer red line due to the existence of vortex, swing toward the inlet direction, section B-5, B-6 tracer streamline swing state similar to section B-4, the tracer red line oscillates upwards in the upper part of the outflow channel, while the tracer red line oscillates downwards in the outflow channel, and there is an obvious stratification of the water flow. This phenomenon can also be found through the previous numerical simulation results, which is due to the formation of backflow vortex caused by the opposite axial velocity of the water flow on the upper and lower side of the outlet channel of the pump gate.

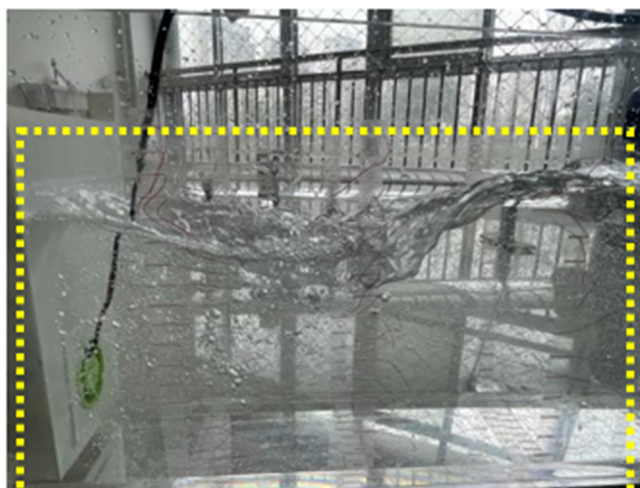


Figure 27. Flow pattern at the outlet of the pump gate guide vane.

5. Conclusions

In this paper, the SST $k-\omega$ turbulence model is used to numerically simulate the integrated pump gate and verify its flow characteristics through experiments, the main conclusions are as follows.

(1) The numerical calculation results show that the efficiency of the integrated pump gate is 60.50% near the designed flow condition, the corresponding flow rate is 11.5 L/s, the head is 2.7569 m, the hydraulic loss of the intake channel is 0.064 m, and that of the outlet channel is 1.337 m.

(2) In this paper, through the axial velocity distribution and streamline of the inlet and outlet channels, combined with the pressure distribution at the inlet and outlet of the pump gate, the flow pattern of the integrated pump gate was analyzed, and it was concluded that the inlet flow pattern of the pump gate was uniform, and there was a large backflow vortex at the outlet of the pump gate. With the increase of the inlet flow, the vortex area increases and the center moves back.

(3) Integrated pump gate test results show that the streamline in the open inlet channel is smooth, parallel to each other, with no cross entanglement phenomenon. Impeller near the inlet, the tracer red line gradually converge to the impeller inlet, gradually contracted, uniform swing, no obvious bad flow pattern, vortex exists at the outlet of guide vane. In the middle and rear section of open outlet channel, the tracer red line gradually returns to parallel, and the streamline near the wall slightly swings upward at the outlet slope. The experimental phenomenon is similar to the numerical calculation result.

Author Contributions: Concept design, C.X. and W.X.; numerical calculation, A.F. and W.X.; experiment and data analysis, A.F. and F.S.; manuscript writing, C.X. and W.X. All authors have read and agreed to the published version of the manuscript.

Funding: This research was funded by Anhui Province Natural Science Funds for Youth Fund Project, grant number 2108085QE220. Key scientific research project of Universities in Anhui Province, grant number KJ2020A0103. Anhui Province Postdoctoral Researchers' Funding for Scientific Research Activities, grant number 2021B552. Anhui Agricultural University President's Fund, grant number 2019zd10. Stabilization and Introduction of Talents in Anhui Agricultural University Research Grant Program, grant number rc412008.

Institutional Review Board Statement: Not applicable.

Informed Consent Statement: Not applicable.

Data Availability Statement: Not applicable.

Conflicts of Interest: The authors declare no conflict of interest.

References

1. Zhao, Q. Analysis of the characteristics and application advantages of integrated pump gate. *Electromechanical Inf.* **2020**, *52*–53. [[CrossRef](#)]
2. Zhou, M.; Meng, F.; Zhang, W. Development and application of an integrated pump gate. *Gen. Mach.* **2014**, *85*–86.
3. Kentaro, F.; Yu, K.; Hiroaki, F. Validation of Inundation Damage Reduction by a Pump Gate with the New Type of Horizontal Axial Submersible Pump. *J. Disaster Res.* **2021**, *16*, 381–386.
4. Chen, W. *Numerical Simulation Study on Hydraulic Optimization of Integrated Pump Gate*; Yangzhou University: Yangzhou, China, 2021.
5. Shi, X.; Yan, G.; Dong, J.; Yang, Y. Safety study and structural optimization of vertical integrated pump gate. *Vib. Test. Diagn.* **2021**, *41*, 176–181+207.
6. Shi, X.; Yan, G.; Dong, J.; Sun, Y. Safety study and structural optimization of horizontal integrated pump gate. *Vib. Shock* **2021**, *40*, 42–47.
7. Wu, Y.; Zhao, H.; Liu, C. Based on The Gate Bottom Edge Structures Specific Numerical Simulation of Flow Pattern of Gate. *E3S Web Conf.* **2021**, *261*, 02018. [[CrossRef](#)]
8. Guo, M.; Chen, Z.; Lee, Y.; Choi, Y.D. Air Entrainment Flow Characteristics of Horizontal and Elbow Type Gate Pump-Sump Models. *KSFJ J. Fluid Mach.* **2019**, *22*, 54–61. [[CrossRef](#)]
9. Chen, H.; Zheng, Y.; Zhou, D.; Shen, P.; Liu, H. Design and development of an eco-gate pump installation based on computational fluid dynamics. *Proc. Inst. Mech. Eng. Part C J. Mech. Eng. Sci.* **2017**, *231*, 2636–2649. [[CrossRef](#)]
10. Jiang, M. *ANSYS Workbench 19.0 Basic Introduction and Engineering Practice*; People's Post and Telecommunications Publishing Company: Beijing, China, 2019.
11. Shi, L.; Yuan, Y.; Jiao, H.; Tang, F.; Cheng, L.; Yang, F.; Jin, Y.; Zhu, J. Numerical investigation and experiment on pressure pulsation characteristics in a full tubular pump. *Renew. Energy* **2021**, *163*, 987–1000. [[CrossRef](#)]
12. Lu, Z.; Xiao, R.; Tao, R.; Li, P.; Liu, W. Influence of guide vane profile on the flow energy dissipation in a reversible pump-turbine at pump mode. *J. Energy Storage* **2022**, *49*, 104161. [[CrossRef](#)]
13. Launder, B.E.; Spalding, D.B. *Lectures in Mathematical Model of Turbulence*; Academic Press: London, UK, 1972.
14. Menter, F.R. *Zonal Two Equation $k-\omega$ Turbulence Models for Aerodynamic Flows*; AIAA-93-2906; AIAA: Preston, CA, USA, 1993.
15. Yang, F.; Zhang, Y.; Yao, Y.; Liu, C.; Li, Z.; Ahmed, N. Numerical and Experimental Analysis of Flow and Pulsation in Hump Section of Siphon Outlet Conduit of Axial Flow Pump Device. *Appl. Sci.* **2021**, *11*, 4941. [[CrossRef](#)]
16. Xie, C.; Tang, F.; Yang, F.; Zhang, W.; Zhou, J.; Liu, H. Numerical simulation optimization of axial flow pump device for elbow inlet channel. *IOP Conf. Ser. Earth Environ. Sci.* **2019**, *240*, 032006. [[CrossRef](#)]
17. Shi, L.; Zhang, W.; Jiao, H.; Tang, F.; Wang, L.; Sun, D.; Shi, W. Numerical simulation and experimental study on the comparison of the hydraulic characteristics of an axial-flow pump and a full tubular pump. *Renew. Energy* **2020**, *153*, 1455–1464. [[CrossRef](#)]
18. Zhang, W.; Tang, F.; Shi, L.; Hu, Q.; Zhou, Y. Effects of an Inlet Vortex on the Performance of an Axial-Flow Pump. *Energies* **2020**, *13*, 2854. [[CrossRef](#)]
19. Ahmed, N.; Fan, Y.; Yiqi, Z.; Tieli, W.; Mahmoud, H. Analysis of the Flow Pattern and Flow Rectification Measures of the Side-Intake Forebay in a Multi-Unit Pumping Station. *Water* **2021**, *13*, 2025. [[CrossRef](#)]
20. Sun, Z.; Yu, J.; Tang, F. The Influence of Bulb Position on Hydraulic Performance of Submersible Tubular Pump Device. *J. Mar. Sci. Eng.* **2021**, *9*, 831. [[CrossRef](#)]
21. Ji, D.; Lu, W.; Lu, L.; Xu, L.; Liu, J.; Shi, W.; Huang, G. Study on the Comparison of the Hydraulic Performance and Pressure Pulsation Characteristics of a Shaft Front-Positioned and a Shaft Rear-Positioned Tubular Pump Devices. *J. Mar. Sci. Eng.* **2021**, *10*, 8. [[CrossRef](#)]